RESEARCH ARTICLE

Estimation of virtual masses for structural damage identification

Jilin Hou[1] (ORCID) | Zhenkun Li[1] (ORCID) | Łukasz Jankowski[2] (ORCID) | Sijie Wang[3]

[1]Department of Civil Engineering & State Key Laboratory of Coastal and Offshore Engineering, Dalian University of Technology, Dalian, China

[2]Institute of Fundamental Technological Research, Polish Academy of Sciences, Warsaw, Poland

[3]Guangzhou Design Institute, Guangzhou, China

Correspondence

Jilin Hou, Department of Civil Engineering & State Key Laboratory of Coastal and Offshore Engineering, Dalian University of Technology, No.2 Linggong Road, 116024 Dalian, China.
Email: houjilin@dlut.edu.cn

Funding information

National Key Research and Development Program of China, Grant/Award Number: 2018YFC0705604; National Natural Science Foundation of China, Grant/ Award Number: 51878118; National Science Centre, Poland, Grant/Award Number: 2018/31/B/ST8/03152; Fundamental Research Funds for the Central Universities, Grant/Award Number: DUT19LK11

Summary

Adding a virtual mass is an effective method for damage identification. It can be used to obtain a large amount of information about structural response and dynamics, thereby improving the sensitivity to local damage. In the current research approaches, the virtual mass is determined first, and then the modal characteristics of the virtually modified structure are identified. This requires a wide frequency band excitation; otherwise the crucial modes of the modified structure might be out of the band, which would negatively influence the modal analysis and damage identification. This paper proposes a method that first determines the target frequency and then estimates the corresponding value of the additional virtual mass. The target frequency refers to the desired value of the natural frequency after the virtual mass has been added to the structure. The virtual masses are estimated by tuning the frequency response peaks to the target frequencies. First, two virtual mass estimation methods are proposed. One is to directly calculate the virtual mass, using the frequency-domain response at the target frequency point only, whereas the second method estimates the mass using a least-squares fit based on the frequency-domain response around the target frequency. Both proposed methods utilize merely a small part of the frequency domain. Therefore, an impulse, a simple harmonic, or a narrow spectral excitation can be used for damage identification. Finally, a numerical simulation of a simply supported beam and experiments of a frame structure and a truss structure are used to verify the effectiveness of the proposed method.

KEYWORDS

damage identification, frequency response, structural health monitoring (SHM), virtual distortion method (VDM), virtual mass

1 | INTRODUCTION

Recently, increasingly more attention has been paid to the safety and durability of structures, owing to the trend of constructing large-scale and complicated civil structures. Structural health monitoring (SHM) aims at providing effective ways to realize rapid warnings and ensuring structural safety. Structural damage identification is one of the most important components of SHM. The fundamental source of information about the structure is its dynamic response, and therefore virtually all damage identification methods in the field of civil engineering essentially strive to extract it

from the data that is informative and sensitive to damage.[1–3] When a structure is damaged, its time- and frequency-domain responses as well as its modal characteristics change. Therefore, damage identification methods are primarily based on the time-domain response,[4–6] frequency-domain response,[7–9] and modal characteristics.[10,11]

The mode-based identification methods use changes in the structural modal parameters, such as the modal frequency, shape, and strain energy, to identify structural damage. Initially, researchers focused on the natural frequencies of the structure to identify damage; then the frequency change before and after the damage was employed and it was suggested that frequency and modal shapes should be combined to identify damage.[12] Hou et al.[13] proposed a sparse damage identification method using natural frequencies and modal shapes, which applied l_1 regularization to identify sparse damage in a large number of structural elements. Strain modes are more sensitive to local damage of structures than deformation modes. Singh et al.[14] used the measured strain response to extract the strain modal shapes and modal frequencies of a structure and used a two-step pseudo-inversion method to identify the stiffness characteristics of the elements and the structural damage. In addition, modal flexibility and modal energy are also widely used. Dinh-Cong et al.[15] proposed a practical two-stage approach for damage assessment in truss structures. In the first stage, an indicator, normalized modal strain energy-based damage index (nMSEBI), is proposed to locate effectively potential damaged elements. In the second stage, the teaching–learning-based optimization (TLBO) algorithm is used as a solver to determine the damage severity of damage sites. Thereupon, the same authors[16] presented an extensive application of the modal kinetic energy change ratio (MKECR) to damage localization and quantification of laminated composite beams and verified the proposed method by a clamped-clamped composite beam and a two-span continuous composite beam under the influence of incomplete mode shapes and various noise level. Guo and Li[17] proposed an identification method based on the equivalent damage index of the modal strain energy and deduced an accurate expression of modal strain energy before and after damage, which could be used to accurately identify the location and extent of the structural damage. Wang et al.[18] proposed a damage identification and localization method for asymmetric building structures based on vibration damage indicators. The modal flexibility and modal strain energy of the structure were used to identify and locate the asymmetric experimental model. Modal shapes are basic characteristic parameters of a structure. Zhao et al.[19] adopted the structural modal shapes extracted from a finite element (FE) model of a reinforced concrete beam and used different types of wavelets for damage identification. Dinh-Cong et al.[20] utilized a model reduction technique (iterated improved reduced system [IIRS]) to develop a reduced order model for optimal sensor placement using Jaya algorithm and then used incomplete modal data from optimized sensor locations to detect and assess any stiffness reduction induced by damage. In 2019, the same authors[21] used lighting attachment procedure optimization (LAPO) algorithm to solve the optimization problem of damage identification, in which a combination of both natural frequencies and modal flexibility changes is considered as a hybrid objective function. In general, mode-based damage identification methods have the advantages of high efficiency and strong robustness. However, in practical engineering, only a few low-order modes of a structure can be obtained, and it is difficult to accurately capture the local damage of the structure by such limited means. Therefore, for accurate damage identification of engineering structures, it is of a large significance to devise methods to extract a large number of modes with a high sensitivity to local damage.

The addition of physical modifications to the structure increases the number of experimental objects sharing the same damage and thus increases the number of available structural modes. In 1992, Nalitolela et al.[22] proposed for the first time a method of adding physical mass or stiffness to a structure and used the modal information of the new structure to update the model. Since then, the method has been continuously developed through several innovations. Cha and De Pillis[23] added known physical masses to a structure and then used the orthogonal conditions of the system eigenvalue problem to identify the damage. Dems and Mroz[24] used additional control parameters (such as mass, support, load, or temperature) in combination with modal, static, and thermodynamic analyses to identify damage. Dinh et al.[25] furthered the approach by using the state space transformation of the eigenvalue problem and extended the algorithm to stiffness identification of beams. Lee and Eun[26] proposed a damage identification method for frame structures based on the frequency response function (FRF) changes due to an additional mass. It is demonstrated that adding physical modifications to the structure can effectively increase the amount and quality of available experimental data. However, due to the limitation of practical engineering conditions, it is often difficult and impractical to install an actual physical mass or stiffness components to the structure.

The methods of adding virtual (instead of physical) parameters have undergone significant developments that help to avoid the tedious work of actual modifications. The virtual distortion method (VDM)[27] is an effective tool for rapid structural reanalysis. Its basic idea is that the response of a damaged structure can be seen as a linear superposition of the original response of the undamaged structure (under the same external load) and the response to certain virtual distortions related to the damage. Therefore, it is not necessary to rebuild the structural model and analyze the entire

structure when the original response is known. Zhang et al.[28] proposed a virtual control system (VCS), which was composed of a control device and self-balanced forces that could adjust the dynamic characteristics of the controlled structure by tuning the VCS parameters. The accuracy of structural damage identification has been enhanced by using the VCS. Hou et al.[29] proposed a damage identification method based on additional virtual masses and the VDM that used the measured excitation and acceleration response to construct the response of the structure with virtual masses. This increased the sensitivity of modes to local substructure damage, thereby improving the accuracy of damage identification. Hou et al.[30] utilized the fact that additional virtual masses can be used to quickly obtain a large amount of structural response information and proposed a damage identification method based on additional virtual masses and Bayesian theory. The problems of insufficient modal information and insensitivity to local damage could be solved in this way, and the probability density function of the damage factor was obtained. The method was verified in a numerical simulation and an experiment involving a three-story frame structure. The method of adding virtual masses can thus not only yield enough modal information sensitive to local damage but also avoid the difficulty of adding real physical components to the structure.

Importantly, most of the above damage identification methods are based on impulse excitation, which, together with structural acceleration response, is used to construct the responses of the new structures with virtual masses. However, the frequency spectrum of the impulse excitation is very wide and contains many high-frequency components. The significant initial oscillations of the corresponding structural accelerations, to some extent, reduce the accuracy of the constructed responses in the actual experiments. On the contrary, simple harmonic excitation or narrow-spectrum excitation can avoid these flaws of impulse excitation. The energy of a simple harmonic excitation is very narrow band, which can improve the accuracy of constructed responses and damage identification. Therefore, to overcome the current limitations of the virtual mass method, this work considers the case in which the target frequency is determined first and investigates how to accordingly determine the additional virtual mass. Finally, damage identification is performed using the target frequency and the determined additional virtual mass.

The remainder of this paper is organized as follows: Section 2 introduces the proposed virtual mass estimation methods based on the frequency response. Section 3 explains the damage identification based on the additional virtual mass. Section 4 verifies the method numerically by using the FE model of a simply supported beam. Finally, Section 5 validates the approach experimentally by applying it to a plane frame and a truss structure. The paper is concluded in Section 6.

2 | ESTIMATION OF VIRTUAL MASSES BASED ON FREQUENCY RESPONSE

2.1 | Basic idea of additional virtual mass method

The method of additional virtual mass uses the measured excitation and acceleration response of the original structure to quickly construct the frequency response of the same structure with an additional mass. The mass matrix, damping matrix, and stiffness matrix of the undamaged structure are denoted by $\mathbf{M}$, $\mathbf{C}$, and $\mathbf{K}$, respectively. If a certain mass is added to the structure, the equation of motion of the modified structure can be expressed in the frequency domain as Equation 1.

$$(\mathbf{M} + \Delta\mathbf{M})\ddot{X}^V(\omega) + \mathbf{C}\dot{X}^V(\omega) + \mathbf{K}X^V(\omega) = Bf(\omega). \tag{1}$$

Assume that the mass is added in only one degree of freedom (DOF) and that the same DOF is used for excitation and measurement. Let $f(\omega)$ and $a(\omega)$ denote, respectively, the fast Fourier transforms (FFT) of the corresponding excitation and the acceleration response of the original structure. The related FRF is $h(\omega) = a(\omega)/f(\omega)$; see an example shown as the red curve in Figure 1. According to the basic theory of virtual mass,[29] Equation 1 is considerably simplified in the considered case of a single affected, excited and measured DOF. After adding a mass m, the acceleration frequency response function $h_v(\omega, m)$ corresponding to the affected DOF can be derived as

$$h_v(\omega, m) = (a(\omega))/((f(\omega) + ma(\omega)) = (h(\omega)/((1 + mh(\omega)). \tag{2}$$
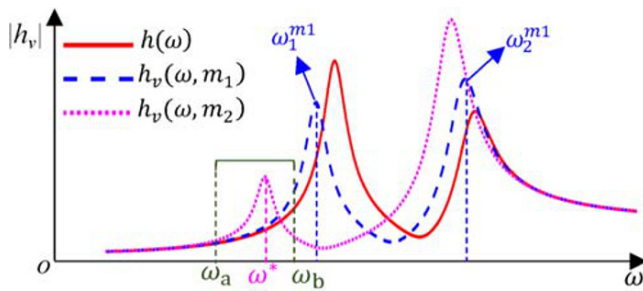
FIGURE 1 Amplitude of the frequency response function: original and for two different additional masses

Given any value of the additional mass m, the corresponding FRF can be straightforwardly calculated, thereby achieving the addition of a virtual mass to the structure without any physical changes to the original structure. In this way, a large number of responses can be quickly constructed after only a single measurement of the real response of the original structure. Equation 2 can be thus used to yield a large amount of information about structural dynamics.

Note that there are two variables in the function $h_v(\omega, m)$, namely, the virtual mass m and the frequency ω, which allows for a certain flexibility in analysis of the resulting FRFs. In the previously proposed approaches, the value of the additional mass was first decided, and then the corresponding structural natural frequencies were determined. Using the example of Figure 1, the specific steps were as follows: the additional mass was decided to be m_1, the corresponding FRF was calculated as $h_v(\omega, m_1)$, and its peaks were used to determine the natural frequencies $\omega_1^{m_1}$ and $\omega_2^{m_1}$ of the structure with the additional mass m_1; see the dashed blue curve in Figure 1. Thereafter, structural damage was identified by using the obtained modal information and combining it with the respective FE models. Such an approach required a physical excitation $f(\omega)$ with a wide spectrum that covered all the structural frequencies of interest to form a relatively complete FRF curve. However, if the spectral range of the excitation $f(\omega)$ was too narrow, such as the spectral range of $[\omega_a, \omega_b]$ in Figure 1, then the peaks of the curve $h_v(\omega, m_1)$ fell outside the frequency interval $[\omega_a, \omega_b]$ and the additional frequency information about the structure could not be reliably determined using the mass m_1.

To avoid such a frequency range limitation, this work proposes and investigates an approach in which the target natural frequency ω^* of the modified structure is decided first, and then the required virtual mass is accordingly determined. As the desired natural frequency ω^* is an independent variable, it can be set within the allowable frequency range, $\omega^* \in [\omega_a, \omega_b]$. The value of the additional mass m_2 is then adjusted to obtain such a frequency response function $h_v(\omega, m_2)$ that reaches the peak value at $\omega = \omega^*$, which is shown as the dotted pink curve in Figure 1. The following two subsections propose a geometric interpretation and two approaches that allows the required additional mass to be quickly determined.

2.2 | Target frequency

In order to estimate the additional virtual masses, the first step is to determine the target natural frequency. Three important points should be taken into account:

1. Natural frequencies of the experimental model without additional virtual masses should be estimated first and then used to determine the target frequencies.
2. The target natural frequency is supposed to be a little smaller than the structural actual frequency. If the target frequency is larger than the actual natural frequency, then the corresponding additional virtual mass has a negative value. However, the additional virtual mass is positive, if the target frequency is smaller than the actual natural frequency. Positive additional masses are found to improve, to a great extent, the sensitivity of the local substructural dynamics to damage.
3. The target frequency cannot be too far from the structural natural frequency. To significantly increase the sensitivity of structural modes to damage, the additional virtual mass is expected to be large. However, in general, due to the influence of noise, the larger the additional mass is, the greater the errors of the constructed responses of the virtual structure. Therefore, the larger the gap between the target frequency and the actual frequency is, the larger the additional mass is and the larger the related errors are. Hence, to ensure the precision of the estimated virtual masses, the target frequency should not be far from the actual natural frequency.

2.3 | Initial direct estimation of the additional virtual mass

Let the target natural frequency be ω^*, and denote by $m^\#$ the corresponding value of the additional virtual mass that is to be determined. This subsection describes a simple first-order approach that can be used for a quick direct estimation of $m^\#$ by using the value of the frequency response $h(\omega^*)$ only at $\omega = \omega^*$.

Given the target excitation frequency $\omega = \omega^*$, the corresponding frequency-domain response of the original unmodified structure is $h(\omega^*)$, and the frequency response corresponding to the additional mass m can be obtained from Equation 2 as $h_v(\omega^*, m)$. The amplitude of the frequency response $|h_v(\omega^*, m)|$ depends on the additional mass m as shown in Figure 2, and the peak point of the curve is P. The initial estimation is the mass $m^\#$ that corresponds to the peak point P: such a choice maximizes the amplitude $|h_v(\omega^*, m)|$ of the frequency response at $\omega = \omega^*$ with respect to m, and thus approximates the desired resonance conditions.

In Equation 2, the mass m is in the denominator, which is not conducive to deriving the analytic expression. Therefore, to facilitate the derivation, instead of maximizing $|h_v(\omega^*, m)|$, one can equivalently minimize its reciprocal $|h_v(\omega^*, m)|^{-1}$. Combined with Equation 2, the following objective function to be minimized is thus established:

$$\Delta(m, \omega^*) = |(1/h(\omega^*)) + m|. \tag{3}$$

The structural frequency response is a complex number, while the mass m is a real number. Let $h(\omega) = \bar{x}(\omega) + \bar{y}(\omega)i$, where $(\bar{x}(\omega)$ and $(\bar{y}(\omega)$ represent the real and imaginary parts of the frequency response $h(\omega)$, respectively. Denote by $\hbar(\omega)$ the reciprocal of the frequency response $h(\omega)$, and let $x(\omega)$ and $y(\omega)$ be its real and imaginary parts: $\hbar(\omega) = 1/h(\omega) = x(\omega) + y(\omega)i$, where $x = \frac{\bar{x}}{\bar{x}^2 + \bar{y}^2}$, $y = -\frac{\bar{y}}{\bar{x}^2 + \bar{y}^2}$. Therefore, for ω^*, $1/h(\omega^*) = x^* + y^*i$, which in Figure 3 is shown as the point $A^*(x^*, y^*)$ of the complex plane. Let the point $B(-m, 0)$ represent the position in the coordinate system that corresponds to the additional mass m, such that the distance $|A^*B|$ is equal to $\Delta(m, \omega^*)$ in Equation 3. From Figure 3, it is obvious that $|A^*B|$ is minimal when $\overrightarrow{BA^*}$ is perpendicular to the x-axis, that is, when point B coincides with point C.

FIGURE 2 Relationship between frequency response amplitude and additional mass
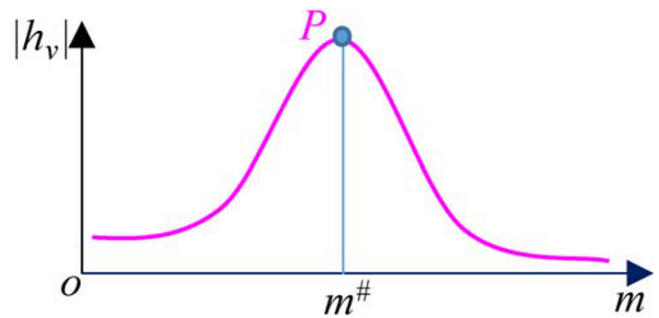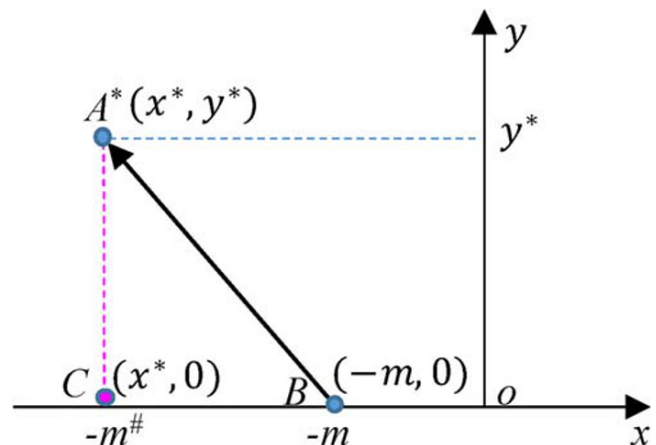
FIGURE 3 Geometric interpretation used for the initial direct estimation of the virtual mass

Therefore, $-m = x^*$, and the frequency response $h(\omega^*)$ at the target point ω^* can directly estimate the additional mass $m^\#$ as in Equation 4.

$$m^\# = -x^* = -\bar{x}^* / \left((\bar{x}^*)^2 + (\bar{y}^*)^2 \right) = -\operatorname{Re} h(\omega^*) / |h(\omega^*)|^2. \tag{4}$$

2.4 | Improved estimation of the additional virtual mass

The curve $|h_v(\omega^*, m)|$, as shown in Figure 2, is in fact a section of a 3D surface $|h_v(\omega, m)|$ at $\omega = \omega^*$, which is shown in Figure 4 as the solid pink line. The peak point P of $|h_v(\omega^*, m)|$ with respect to the mass corresponds to the additional mass $m^\#$. However, when the virtual mass $m^\#$ is added to the structure, the actual frequency response $|h_v(\omega, m^\#)|$ with respect to the frequency ω is shown as the dashed blue line in Figure 4. The peak position of this curve is $P^\#$, and the position of the corresponding natural frequency is $\omega^\#$. Generally, the points P and $P^\#$ are close to each other, but they are not the same point; that is, the natural frequency $\omega^\#$ only approximates ω^* when the additional mass $m^\#$ is added. Assume that the natural frequency equals ω^*, when the added mass is m^*; see the dotted purple line in Figure 4 with the peak point P^*. Therefore, when only one point of the frequency response $|h(\omega^*)|$ at ω^* is used, the estimated virtual mass $m^\#$ generally only approximates the desired mass m^*. The accuracy of the estimated virtual mass can be improved by taking into account the frequency response also in the neighborhood of ω^*.

The dependence of the reciprocal $\hbar(\omega)$ of the original structural frequency response on the frequency ω is shown in Figure 5 as the solid green line in the complex plane. Point A^* indicates the position of the complex number $1/h(\omega^*)$ in the coordinate system. The additional virtual mass m corresponds to point $B(-m, 0)$ in the figure, so that the distance $|BA^*|$ equals $\Delta^* = \Delta(m, \omega^*)$. As the virtual mass m changes, the point B moves along
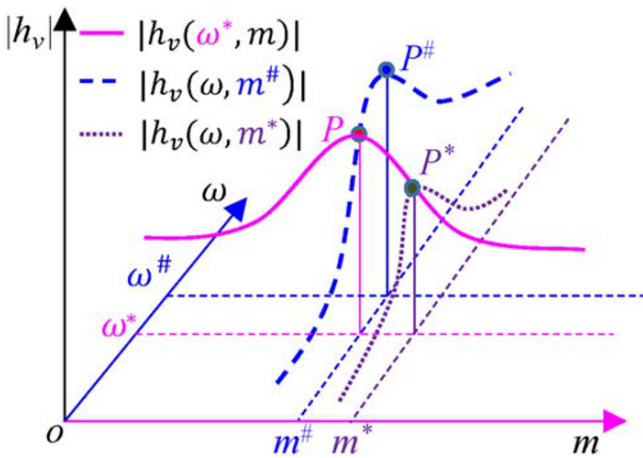

FIGURE 4 Relationship between the frequency response amplitude and the additional mass
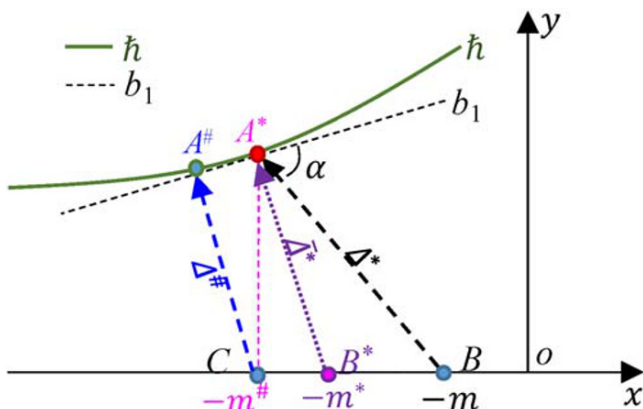
FIGURE 5 Reciprocal of the frequency response function in the complex plane and improved determination of the additional mass

the horizontal axis. Point $C(-m^{\#}, 0)$ in Figure 5 is the virtual mass directly estimated by using the frequency response corresponding to the point A^*, as shown also in Figure 3. However, the distance $|BA^*|$ needs to be minimum with respect to the frequency ω, that is, with respect to the solid green line in the neighborhood of A^*. Let the straight dashed line b_1 be the tangent of the curve at point A^*. The point of intersection between the normal at point A^* on the curve $\hbar$ and the horizontal x-axis is point B^*. Let the coordinates of B^* be $(-m^*, 0)$, where A^*B^* is the shortest distance from B^* to the curve $\hbar$. Point C corresponds to the added mass $m^{\#}$, and the shortest distance from point C to the curve $\hbar$ is $|A^{\#}C|$. That is, the corresponding point to the added mass $m^{\#}$ is $A^{\#}$ rather than the target point A^*. The slope of the tangent line b_1 is $\bar{y}'$. Then, according to the geometric relationship in Figure 5, m^* and $\bar{\Delta}^*$ can be obtained from Equations 5 and 6.

$$m^* = -x^* - y^* \bar{y}', \tag{5}$$

$$\bar{\Delta}^* = |y^*| \sqrt{1 + (\bar{y}')^2}. \tag{6}$$

In the following, it is analyzed whether m^* is the required additional mass, that is whether $|B^*A^*|$ is indeed the shortest distance between point B^* and $\hbar$. Let the derivative of $\hbar$ be $\bar{y}'$ and the curvature radius of $\hbar$ be R^*. The curvature radius R^* is expressed by Equation 7.

$$R^* = \left(1 + \bar{y}'^2\right)^{3/2} / |\bar{y}''|. \tag{7}$$

The analysis is divided into the following two cases as Figure 6 shows:

1. When $\bar{y}'' y^* \geq 0$, as exemplified by curve $\hbar_1$ in Figure 6, then $|B^*A^*|$ is the shortest distance from point B (moving on the x-axis) to curve $\hbar_1$, and m^* is the expected additional mass. The natural frequency of the structure with the additional mass m^* is exactly ω^*.
2. When $\bar{y}'' y^* < 0$, let curve b_2 be a circle with the origin B^* and the radius $\bar{\Delta}^*$, so the curvature radius of b_2 is obviously $\bar{\Delta}^*$. When the curvature radius R^* of $\hbar$ is larger, as exemplified by curve $\hbar_2$, that is, when $R^* > \bar{\Delta}^*$, then the curve $\hbar_2$ in Figure 6 is located between b_1 and b_2. In such a case, $|B^*A^*|$ is still the shortest distance from B^* to curve $\hbar_2$, and m^* is the additional mass sought. However, when the curvature radius $R^* \leq \bar{\Delta}^*$, as exemplified by curve $\hbar_3$, then $|B^*A^*|$ is the longest distance from B^* to curve $\hbar_3$ and m^* is not the required additional mass: the virtual mass cannot be estimated under such conditions. It is recommended that other frequencies are selected for the estimation.

After analyzing the above conditions, through a simple derivation, the judgment condition of Equations 8–10 can be obtained. That is, if the curve $\hbar$ satisfies $\Gamma(A^*) > 0$ at point A^*, then there is a virtual mass m^* that makes the natural frequency of the structure equal to ω^*; otherwise, there is no such a virtual mass, and it is recommended that the target frequency is changed.
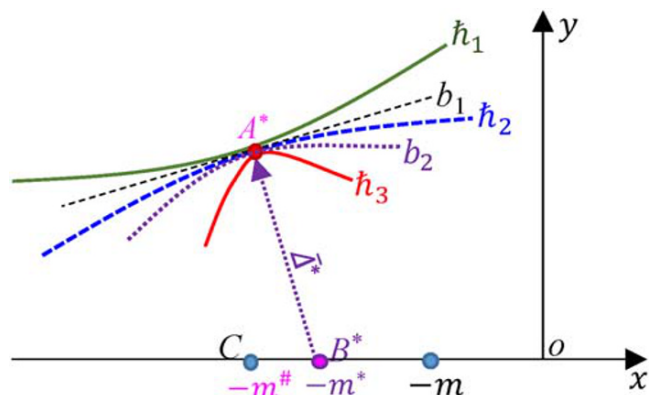

FIGURE 6 Relationship between curvature and virtual mass

$$m = \begin{pmatrix} m^* & \text{if } \Gamma(\text{A}^*) > 0 \\ \text{NaN} & \text{if } \Gamma(\text{A}^*) \leq 0 \end{pmatrix}, \tag{8}$$

$$\Gamma(\text{A}^*) = \frac{\bar{\Delta}^*}{R^*} + 1 = \frac{\text{sign}(y^*)\bar{y}'' \bar{\Delta}^*}{\left(1 + \bar{y}'^2\right)^{3/2}} + 1, \tag{9}$$

$$\text{sign}(y^*) = \begin{pmatrix} 1, & y^* > 0 \\ 0, & y^* = 0 \\ -1, & y^* < 0 \end{pmatrix}. \tag{10}$$

By comparing Equations 4 and 5, it is noticed that the improved method adds a correction term $-y^*\bar{y}'$ and it judges whether the virtual mass can be obtained. In this way, when the target frequency of the structure is unreasonable, another frequency can be selected according to the judgment conditions. After adding the correction term of the additional mass, the estimation of the additional mass value of the structure is more accurate, which is more conducive to the damage identification of the structure.

2.5 | Virtual mass estimation using experimental data

Because the actual measured response is always affected by noise, the calculated frequency response at A^* may have errors. The normal to the curve $\hbar$ cannot be determined accurately. Therefore, available data of the frequency response near A^* are used for the estimation. A fitting method is used to obtain the value of the curve at A^* and the corresponding first and second derivatives, which can improve the estimation accuracy of the virtual mass.

Assume that the data near A^* are the measured frequency response $h(\omega_i)$ corresponding to the frequencies $\omega_1, \omega_2, \cdots, \omega_n$, and the reciprocal of the frequency response $\hbar(\omega_i)$ corresponding to frequency ω_i is the point A_i in Figure 7. The real part of $\hbar(\omega_i)$ is x_i and the imaginary part of $\hbar(\omega_i)$ is y_i, where $i = 1, 2, \cdots, n$. The actual relationship between y_i and x_i in $\hbar(\omega_i)$ is shown by the curve in Figure 7. If the real part x_i and the imaginary part y_i in Figure 7 were directly used to fit the relationship between x and y ($i = 1, 2, \cdots, n$), then the relationship between points on the curve and the frequency ω would be lost. Therefore, in this work, the real part x_i and imaginary part y_i of $\hbar(\omega_i)$ are fitted to ω_i ($i = 1, 2, \cdots, n$). The relationships $x = x(\omega)$ and $y = y(\omega)$ between the real and imaginary parts x and y and the frequency ω are established. Then, the relationship between $x(\omega)$ and $y(\omega)$ is used to calculate the value of A^* and the corresponding first and second derivatives.

Because the points A_i ($i = 1, 2, \cdots, n$) are near A^*, $\hbar(\omega)$ can be modeled as a quadratic curve in the range of $[\omega_1, \omega_n]$. According to the method of least squares, the fitted curves of $x(\omega)$ and $y(\omega)$ can be obtained by Equation 11, where $\mathbf{W}$, $\mathbf{x}$, and $\mathbf{y}$ are as shown in Equation 12 and $\mathbf{W}^+$ represents the generalized inverse of $\mathbf{W}$, which can be calculated using the singular value decomposition.
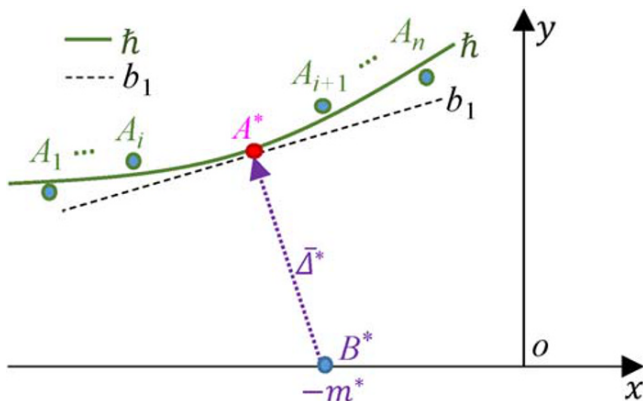

FIGURE 7 Reciprocal of the measured frequency domain response

$$\begin{cases} x(\omega) = [\omega^2 \ \omega \ 1]\mathbf{W}^+\boldsymbol{x} \\ y(\omega) = [\omega^2 \ \omega \ 1]\mathbf{W}^+\boldsymbol{y}' \end{cases} \tag{11}$$

$$\mathbf{W} = \begin{bmatrix} \omega_1^2 & \omega_1 & 1 \\ \omega_2^2 & \omega_2 & 1 \\ \vdots & \vdots & \vdots \\ \omega_n^2 & \omega_n & 1 \end{bmatrix}, \boldsymbol{x} = \begin{bmatrix} x_1 \\ x_2 \\ \vdots \\ x_n \end{bmatrix}, \quad \boldsymbol{y} = \begin{bmatrix} y_1 \\ y_2 \\ \vdots \\ y_n \end{bmatrix}. \tag{12}$$

With $x(\omega)$ and $y(\omega)$ in Equation 11, $y'(x)$ and $y''(x)$ can be calculated as shown in Equations 13 and 14.

$$y'(x) = \frac{y'(\omega)}{x'(\omega)}, y''(x) = \frac{(y''(\omega))}{(x'(\omega))^2} - \frac{(y'(\omega)x''(\omega))}{(x'(\omega))^3}, \tag{13}$$

$$\begin{cases} y'(\omega) = [2\omega \ 1 \ 0](\mathbf{W}^+\boldsymbol{y}) \\ x'(\omega) = [2\omega \ 1 \ 0](\mathbf{W}^+\boldsymbol{x}) \\ y''(\omega) = [2 \ 0 \ 0](\mathbf{W}^+\boldsymbol{y}) \\ x''(\omega) = [2 \ 0 \ 0](\mathbf{W}^+\boldsymbol{x}) \end{cases}. \tag{14}$$

By substituting $\omega = \omega^*$ into Equation 11, x^* and y^* can be calculated, and the initial direct estimation of the additional mass $m^{\#}$ can then be obtained using Equation 4. Furthermore, by substituting $\omega = \omega^*$ into Equations 13 and 14, the derivative $\bar{y}'$ and the second derivative $\bar{y}''$ of the fitted curve can be acquired. Therefore, the accurate virtual mass m^* can be obtained according to Equation 5, and Equation 8 can be used to determine if the virtual mass exists.

3 | DAMAGE IDENTIFICATION BASED ON ADDITIONAL VIRTUAL MASS

3.1 | Rapid determination of damage based on a single virtual mass

There are two cases that the damage can be directly identified using a single estimated mass:

1. If there is only one damage parameter to be identified, then (under a constant target frequency) a direct relationship between the damage extent and the estimated mass can be established for damage identification.
2. Even if there are several unknown damage parameters, the additional virtual mass placed at a specific location of the structure can make a natural frequency sensitive predominantly to a single local damage parameter, so that the estimated virtual mass can be used for a direct identification of the local damage. For an example of a bar in a truss structure, see Hou et al.[31]

Consider a model case, which is a single-DOF system. Assume the mass is M, the stiffness is K, and $\mu \in [0,1]$ is the structural damage factor, defined as the ratio of the stiffness after damage to the stiffness before damage. The natural frequency ω^* is related to the additional mass m^* as follows:

$$\omega^* = \sqrt{\mu K/(M + m^*)}. \tag{15}$$

Therefore, the additional virtual mass m^* of such a single-DOF structure is related to the assumed target frequency ω^* and the damage factor μ as shown in Equation 16:

$$m^*(\mu) = \mu K/(\omega^*)^2 - M. \tag{16}$$

From Equation 16, it can be seen that for a constant target frequency ω^*, the virtual mass $m^*(\mu)$ is linearly proportional to the damage factor μ. When $\mu = 1$, the structure is not damaged, and the required additional virtual mass m^* is

the largest. The more damaged is the structure, the smaller is the value of μ, and the smaller is the additional virtual mass.

For a multi-DOF structure, there is not such a simple linear expression as Equation 16 between the virtual mass m^* and the structural damage factor μ, but the general character of the dependence is preserved: the larger the structural damage (the smaller the value of μ), the smaller is the required additional mass m^*. Therefore, it can be quickly determined whether the structure is damaged by tracing the value of the additional mass.

3.2 | Damage identification based on multiple additional virtual masses

In the cases discussed in Section 3.1 (a single damage or a predominant sensitivity to a single damage), the value of a single additional mass can be used to quickly assess the damage. However, in general, there are multiple damage factors with diversified influence on the natural frequencies, so that several virtual masses should be added at various positions to the structure to obtain more modal information for damage identification. The additional masses are computed by using different target frequencies and different excitation/measurement points.

In the general case, the process of damage identification is as follows: In an example of Figure 8A, the excitation $f(\omega)$ is applied at a certain position, and the acceleration FRF is recorded as $h(\omega)$. By Equation 2, the corresponding FRF with an additional mass m is $h_v(\omega, m)$; see Figure 8B. The direct and/or improved estimation methods are used to obtain the virtual masses corresponding to a number of target natural frequencies ω_{ki}^*, where k indexes the frequencies and i denotes the position of the excitation, measurement, and the mass. In Figure 9, assuming that the first two order target natural frequencies are ω_{11}^* and ω_{21}^*, the corresponding masses m_{11} and m_{21} added to position ① can be calculated. Similarly, the masses m_{12} and m_{22} corresponding to the first two order target natural frequencies ω_{12}^* and ω_{22}^* are obtained when the mass is added to the second position. Such a process is repeated for all positions i, and the masses corresponding to the first two order natural frequencies ω_{1i}^* and ω_{2i}^* are obtained. The objective function for damage identification is established as shown in Equation 17, and the collected information is used to identify the damage location and degree by optimizing the vector $\boldsymbol{\mu}$ of all the damage factors.

$$\Delta = \sum_{k,i} \frac{\left(\omega_{ki}(\boldsymbol{\mu}, \boldsymbol{m_{ki}}) - \omega_{ki}^*\right)^2}{\left(\omega_{ki}^*\right)^2}. \tag{17}$$
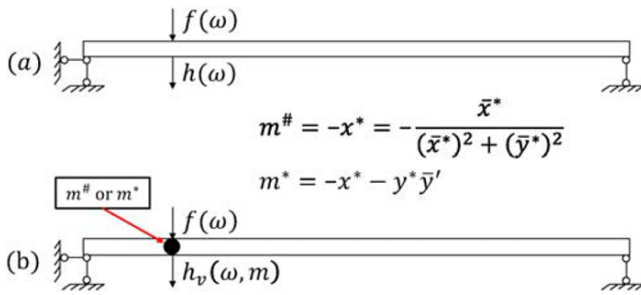

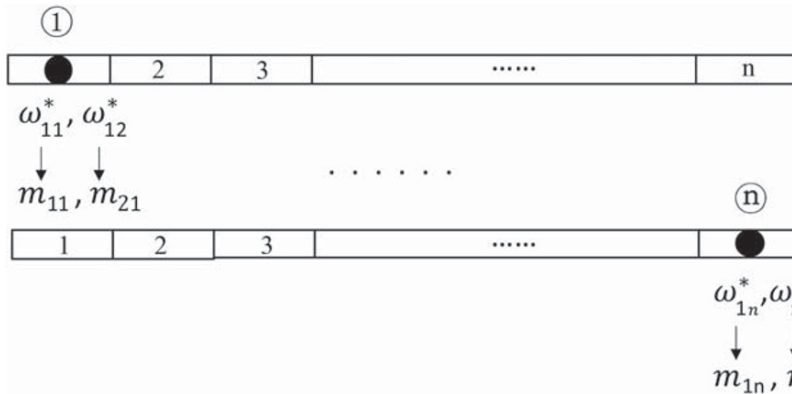FIGURE 8   Adding a virtual mass to a structure

FIGURE 9   Sequential adding of virtual masses

4 | NUMERICAL SIMULATION AND ANALYSIS

4.1 | FE model

To verify the effectiveness of the direct and the improved estimation methods of the additional mass proposed in this work and the feasibility of damage identification using the obtained additional masses, a simple supported beam is used as an example for numerical simulation and analysis. A comparison is offered between the theoretical and calculated values. The specific parameters of the simply supported beam are as follows.

The model adopts a rigid simply supported beam of a constant cross-section, as shown in Figure 10. Its elastic modulus is $E = 210$ GPa, the density is $\rho = 7{,}850$ kg/m^3, Poisson's ratio is 0.3, the length is 1 m, the cross-section width is 0.05 m, and the cross-section height is 0.003 m. The beam is divided into 20 elements and 10 substructures, each of which includes two elements. The nodes between any two adjacent elements are the possible positions of the additional virtual mass. Virtual mass can be thus added to a total of 19 nodes; see Figure 10. According to the theoretical FE model, the first three natural frequencies of the original simply supported beam can be obtained as 7.04, 28.14, and 63.3 Hz.

4.2 | Additional virtual mass and structural frequency

The seventh node is excited and measured in the vertical direction, as shown in Figure 10. The corresponding vertical acceleration frequency response is $H_{77}(\omega)$, and its amplitude is shown in Figure 11 as the curve "Frequency response." The frequency response of the structure can be expressed as the superposition of the frequency responses of its modes. The curves "Mode 1," "Mode 2," and "Mode 3" in Figure 11 are the frequency responses calculated for the first-, second-, and third-order modes, respectively.

By substituting $H_{77}(\omega)$ into Equation 4, a directly estimated value $m^{\#}(\omega)$ of the virtual mass at Position 7 can be obtained for each target frequency ω, which is shown by the $m^{\#}$ curve in Figure 12. To determine the accurate value of $m^*(\omega_i)$, seven points of the frequency response near each ω_i are selected as $\omega_{i-3}, \omega_{i-2}, ..., \omega_{i+3}$ with 0.008-Hz separation.

FIGURE 10 Simply supported beam model and the division into elements

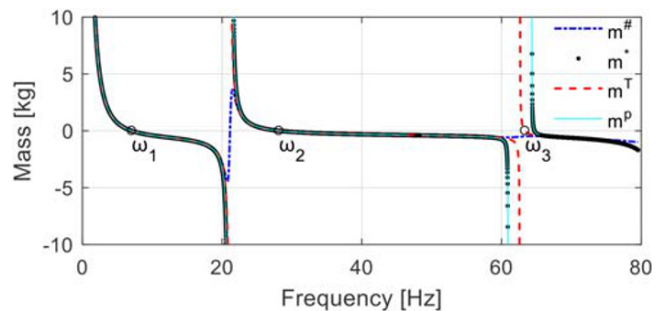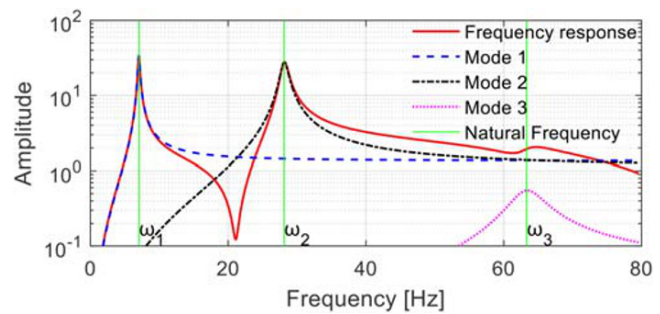**FIGURE 11** Frequency response of the investigated beam

FIGURE 12 Relationships between the additional virtual mass at position 7 and the natural frequencies

The values of the seven points are substituted into Equations 11–14, and the improved estimation of the additional virtual mass is shown as the m^* curve in Figure 12. These curves are obtained based on the FRF of the original structure using the methods proposed in Section 3. They are compared with the results obtained based directly on the FE model: an additional mass in the range of $[-10,10]$ kg is added in the FE model at Position 7. The curve m^T in Figure 12 denotes the relation between the additional mass and the FE-based first three natural frequencies of the beam. Finally, the curve labeled m^P is obtained by peak-picking from the FE-based FRF.

From Figures 11 and 12, the following conclusions can be drawn:

1. There is an intuitive inverse relation between the natural frequency of the structure and the additional mass. The smaller the target natural frequency of the structure, the larger the additional mass.
2. For the target frequency near the structural resonances (natural frequencies), the additional mass is expectably near zero and relatively insensitive to the target frequency. In contrast, near antiresonances, the determined curves are discontinuous and the additional mass is highly sensitive to the target frequency.
3. The virtual mass $m^{\#}$ obtained by the direct estimation method is continuous near antiresonances, which is inconsistent with the actual law (curve m^T), and the error is significantly large. However, the method is relatively accurate for the target frequencies in-between the antiresonances and especially near dominant resonances of the structure.
4. The improved method can accurately obtain the virtual mass corresponding to the peak frequency of the FRF (the curves m^* and m^P coincide). Due to the influence of damping, the peak position of the frequency response is often different from the exact natural frequency. There is thus a certain error between the frequency corresponding to the peak point and the natural frequency, so that the curves m^* and m^T do not exactly overlap. The virtual mass m^* obtained by the improved method is properly discontinuous near antiresonances. The accuracy of the improved estimation method is thus higher than that of the direct estimation method.

4.3 | Virtual mass estimation

The methods proposed in this work may adopt impulse excitation or simple harmonic excitation. The time-domain response must be accurately measured. Impulse excitation had been used to construct additional virtual mass in previous studies. Here, a simple harmonic excitation is used to conduct a numerical simulation to verify the feasibility of the proposed methods.

A harmonic burst excitation is applied vertically at the seventh position of the beam. The excitation frequency is $\omega_f = 25$ Hz, which is close to the second-order natural frequency of the structure. The action time is $T_f = 0.82$ s, and the load is selected as in Equation 18.

$$f(t) = \frac{\left(1 - \cos\left(\frac{2\pi t}{T_f}\right)\right)\sin(2\pi\omega_f t)}{2} \quad \text{for } t \in [0, T_f]. \tag{18}$$

When the excitation is applied, 5% noise is added to model the influence of environmental noise. The excitation time history is shown in Figure 13, and the response time history calculated by the FE model is shown in Figure 14. To perform calculations using the proposed methods, the excitation and response time histories must be analyzed in the frequency domain. The Fourier transforms of the excitation and response are calculated.
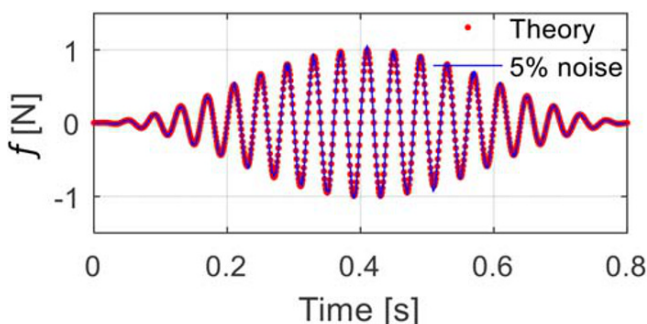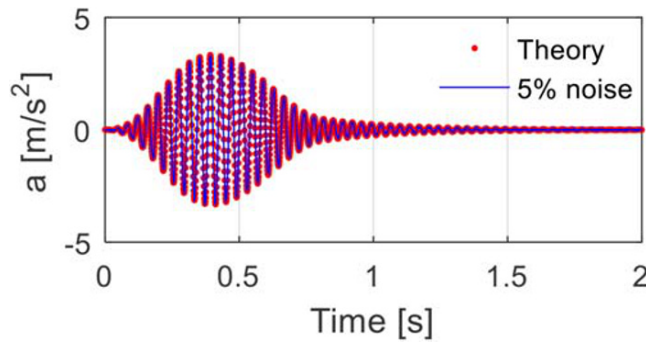

FIGURE 13 Excitation

FIGURE 14   Response

The target frequency of the modified structure is assumed to be 25 Hz. The data in the range of 24.5–25.5 Hz is selected to estimate the additional mass. The data presented in Figures 15 and 16 are used to calculate the frequency response $h(\omega)$ of the structure. The real and imaginary parts of its reciprocal $\hbar(\omega)$ are fitted with respect to the frequency as described in Section 2.4 and shown in Figure 15. Using the fitted data, the direct estimation method yields the estimated additional mass as 0.33637 kg, whereas the improved method yields the virtual mass of 0.36275 kg. These two masses are used to modify the original structural model to obtain the corresponding second-order natural frequencies of the structure, which are 25.09 and 24.96 Hz, respectively. According to the theoretical FE model, when the second-order natural frequency of the structure is 25 Hz, the actual additional mass should be 0.35507 kg. The above results show that both the direct and the improved methods estimate the value of the additional virtual mass; however, the improved method yields more accurate estimations.

To analyze the effect of noise randomness, thirty 5% noise histories are independently generated and sequentially added to the excitation and response. The mean and standard deviation of the estimated additional mass and the resulting frequency are calculated by using the direct and improved estimation methods; see Table 1. The relative error of the additional mass obtained by the direct estimation method is approximately 5.2%, whereas the relative error

FIGURE 15   Relation between the real part and the imaginary part of $\hbar(\omega)$
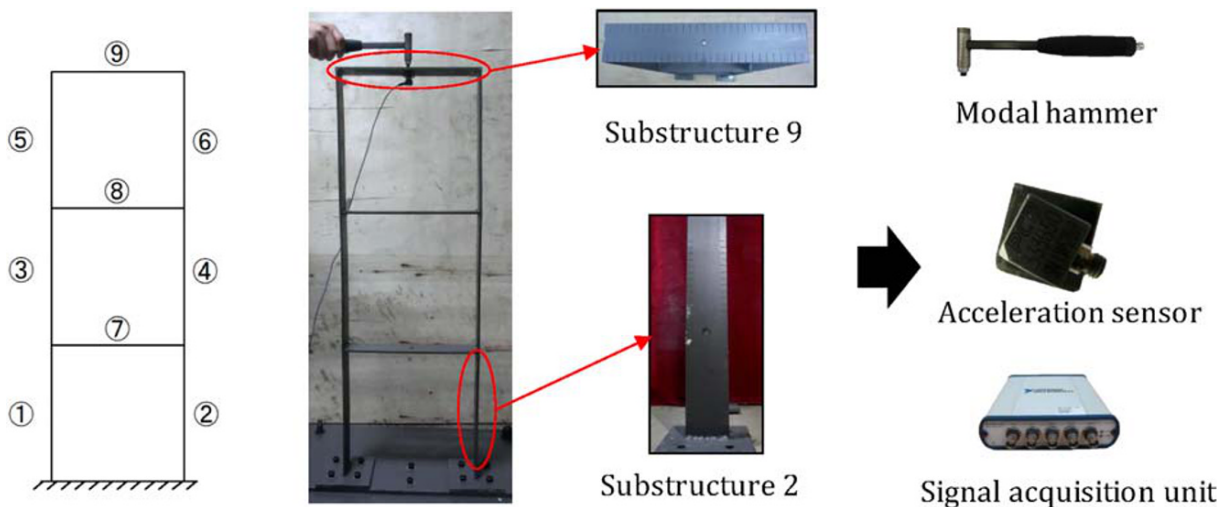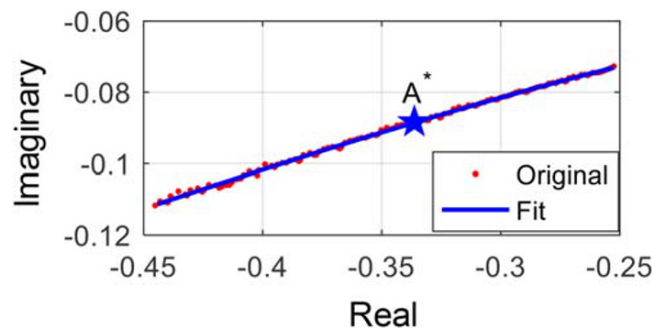

FIGURE 16   Experimental model

between the corresponding second-order natural frequency of the structure is approximately 0.38%. The improved estimation method decreases the relative error of the additional mass to 2.18% and the relative error of the corresponding second-order natural frequency to 0.15%. The improved estimation method yields better results that are less affected by noise.

4.4 | Structural damage identification

The original beam structure is divided into 10 substructures, each of which contains two elements, as shown in Figure 10. It is assumed that the third and sixth substructures of the structure are damaged by reducing their stiffness, and the damage factors are 0.6 and 0.7, respectively. The actual damage factor of the structure can be thus expressed as the vector $\mu = [1,1,0.6,1,1,0.7,1,1,1,1]$. According to the structural FE model, the first three natural frequencies after the damage can be calculated as 6.56, 26.38, and 59.86 Hz.

The target and excitation frequencies selected here are 2, 4, 22, and 53 Hz, which corresponds to the first, first, second, and third natural frequencies of the structure, respectively. The excitation effective time is $T_f = 0.82$ s. Nineteen nodes of the beam are sequentially selected to add a virtual mass; see Figure 10. In each node, four simple harmonic excitations signals are exerted at the target frequencies of 2, 4, 22, and 53 Hz, and then the structural responses are calculated. In the entire process, 5% white noise is considered. The direct and improved estimation methods are used to obtain the additional mass values: the 2-, 4-, 22-, and 53-Hz excitations are applied on each node respectively, and the mass can be estimated according to the target frequencies. For example, when the excitations are applied on node 3, additional masses can be calculated as 21.45, 95, 0.38, and 0.23 kg by the direct estimation method according to 2-, 4-, 22-, 53-Hz harmonic excitations. For the improved estimation method, additional masses are calculated as 21.46, 95, 0.39, and 0.28 kg according to 2-, 4-, 22-, 53-Hz harmonic excitations.

Additionally, after the excitations are applied on all nodes, respectively, it shows that some estimated additional virtual masses may be negative. For instance, when the 22-Hz harmonic excitation is applied on Node 8, the estimated mass is −28.24 kg. This happens when the position of the excitation is close to the node of the respective modal shape, and the corresponding mode of the structure is hardly excited, which causes problems in the estimation of the additional mass. Therefore, this part of the data are eliminated, and only the remaining mass values are used for damage identification. The results are shown in Table 2, separately for the masses obtained by the direct and the improved estimation method.

It can be seen from Table 2 that the identification results obtained by the improved virtual mass estimation method are closer to the real values. The errors are smaller, and there is no misjudgment of the ninth substructure as by the direct estimation method. The results of the numerical simulation confirm that it is feasible to first select the target structural frequency and then to determine accordingly the additional mass for damage identification, and that the improved mass estimation method is more effective.

TABLE 1 Mean and standard deviation of the additional mass and the related structural frequency

	Additional mass (kg)		Structural frequency (Hz)	
	Mean	Standard deviation	Mean	Standard deviation
Direct estimation method	0.3364	0.00325	25.09	0.0169
Improved estimation method	0.3628	0.00149	24.96	0.0072
Theoretical FE-based values	0.3551	—	25.00	—

Abbreviation: FE, finite element.

TABLE 2 Structural damage identification results

No. of substructure	1	2	3	4	5	6	7	8	9	10
Direct estimation method	1.00	1.00	0.52	1.00	1.00	0.78	1.00	1.00	0.92	1.00
Improved estimation method	1.00	1.00	0.62	1.00	1.00	0.64	1.00	1.00	1.00	1.00
Theoretical damage extent	1.00	1.00	0.60	1.00	1.00	0.70	1.00	1.00	1.00	1.00

The following part considers a case of a triple damage with significantly different damages extents. It is assumed that the damage factors of the third, sixth, and eighth substructures are 0.9, 0.4, and 0.1, respectively. According to the structural FE model, the first three natural frequencies of the damaged structure are 4.68, 19.71, and 48.90 Hz. Then, the target frequencies are set as 1.5, 3, 12 and 44 Hz, which corresponds to the first, first, second, and third natural frequencies of the structure, respectively. In the entire process, 5% noises are considered. The results of damage identification are shown in Table 3, as calculated based on the two virtual mass estimation methods described above.

It can be seen from Table 3 that when the damage extent increases, the overall accuracy of damage identification decreases. Damage identification results using the direct estimation method has more mistakes than the results using the improved estimation method. Even in the case of the improved estimation method, the third substructure with damage the factor of 0.9 cannot be identified, and the fifth substructure is wrongly identified as a damaged substructure. So the damage identification precision will decrease with the increase of practical damage.

5 | EXPERIMENTAL STUDY

5.1 | Frame model

In this part, the proposed virtual mass estimation method is verified in damage identification of a plane frame structure. The experimental frame model and its FE model are described in detail in Hou et al.[30] Here, the novel method mentioned above is used to conduct damage identification.

5.1.1 | Experimental stand

As shown in Figure 16, a three-story plane frame model is manufactured to conduct damage identification.[30] The basic parameters of the plane frame after the model is updated are shown in Table 4. The frame is divided into nine substructures. The experimental devices include a modal hammer, an acceleration sensor, and a signal acquisition unit. Modal hammer is adopted in this experiment to apply the excitation due to its unique attributes of convenience, feasibility, and speed.

The damage is simulated by multiple incisions in the frame structure. In particular, the damage is made on both sides of Substructure 2 to simulate its uniform stiffness decrease of approximately 29% (calculated based on the updated numerical models before and after damage). Similarly, stiffness of Substructure 9 is decreased by approximately 46%. Thus, the actual damage factors of the frame structure are $\mu = [1, 0.71, 1, 1, 1, 1, 1, 1, 0.54]$.

5.1.2 | Determination of the target frequency

The FE models of actual structures usually have some modeling errors as compared with the experimental structure. The FE model of the frame structure was precisely built and tuned to the experimental frame structure. The tuning process is described in Hou et al.[30] and its accuracy level can be assessed by the comparison of the natural frequencies after

TABLE 3 Structural damage identification results of a triple damage

No. of substructure	1	2	3	4	5	6	7	8	9	10
Direct estimation method	0.93	1.00	0.92	1.00	1.00	0.51	1.00	0.09	0.80	1.00
Improved estimation method	1.00	1.00	1.00	1.00	0.92	0.44	1.00	0.08	1.00	1.00
Theoretical damage extent	1.00	1.00	0.90	1.00	1.00	0.40	1.00	0.10	1.00	1.00

TABLE 4 Basic parameters of the frame structure

Parameter	Frame height	Frame width	Young's modulus	Density	Sectional width	Sectional thickness
Value	0.3 m	0.295 m	1.94 GPa	7850 kg/m³	0.06 m	0.005 m

1.5 kg mass is added to each substructure between the FE model and the experimental structure, which for the fourth natural frequency is shown in Table 5.[30]

The sensitivity of different order frequencies to damage of each substructure with an added mass is different. By the sensitivity analysis,[30] the fourth-order natural frequency is found to be sensitive to local damage. Therefore, it is selected to determine the target frequency for damage identification. The fourth-order frequency of the intact FE model ω_{ua} is calculated as 132.67 Hz. For the intact FE model, the added virtual mass m of each substructure and the corresponding fourth-order frequency ω_a after adding the mass are, respectively, shown in the "Added mass" and "ω_a" rows of Table 6. Considering Substructure 1 as an example, if 1.5 kg is added at the center of Substructure 1, the fourth-order frequency becomes 110.63 Hz.

In Hou et al.[30] the additional masses (see Table 6 "Added mass") are defined arbitrarily in advance. However, if the frequencies "ω_a" obtained for the intact structures are used with the damaged structure to determine the additional virtual masses using the proposed methods, it will cause the estimated masses to be too small to affect and improve considerably the sensitivity of the substructures. For example, the fourth-order natural frequency of the damaged structure is 122.26 Hz and very close to the fourth-order natural frequency of the intact structure with 1 kg mass added to the second substructure (120.45 Hz). If the target frequency of 120.45 Hz was used, the mass would be significantly small and could not induce a high sensitivity to local damage. Therefore, a decrease factor k is used to determine the target frequency by requiring that the frequency decrease for the damaged structure is the same as for the intact structure:

$$k \approx \omega_a / \omega_{ua}. \tag{19}$$

Through structural dynamic experiments, the fourth-order natural frequency of the damaged structure can be determined as 122.26 Hz. This value is used with the decrease factor k to determine the target frequencies for the damaged structure, as shown in Table 6 "The target frequency."

In the experiment, the excitation is sequentially applied to every substructure, and the corresponding response is obtained. The actual excitation and acceleration response for Substructure 1 are shown in Hou et al.[30] The sampling frequency is 10,000 Hz.

TABLE 5 The fourth natural frequency of FE models and the experimental model after 1.5 kg is added to each substructure

	Substructures								
Model of the structure	**1**	**2**	**3**	**4**	**5**	**6**	**7**	**8**	**9**
Initial FE model	113.84	113.84	105.24	105.24	99.83	99.83	86.59	84.27	82.31
Tuned FE model	110.63	116.03	102.38	102.38	97.21	97.21	84.84	82.56	80.77
Experimental model	109.80	109.20	101.70	101.90	97.66	97.46	81.66	81.16	80.50

Abbreviation: FE, finite element.

TABLE 6 Added mass on different substructures

	Substructure	**1**	**2**	**3**	**4**	**5**	**6**	**7**	**8**	**9**
Intact FE model (fourth-order frequency ω_{ua} = 132.67 Hz)	**Added mass (kg)**	1.5	1	2	2	1.5	1.5	1	1	0.5
	ω_a (Hz)	110.63	120.45	97.47	97.47	97.21	97.21	97.96	94.69	104.98
	Freq. decrease factor k	0.83	0.91	0.73	0.73	0.73	0.73	0.74	0.72	0.79
Damaged model (fourth-order frequency: 122.26 Hz)	The target frequency (Hz)	100	110	90	90	90	90	93	87	97
	$m^{\#}$ (kg)	2.0461	0.8513	2.3772	2.0319	1.7054	1.5607	1.1156	1.0694	0.3298
	m^{*} (kg)	2.1239	0.8545	2.3836	2.0485	1.7115	1.5888	1.0892	1.0656	0.3315

Abbreviation: FE, finite element.

For the entire experiment, nine sets of excitation and acceleration responses are recorded (one for each substructure). To decrease the influence of the measurement noise, every set consists of three groups of experimental data including an excitation and acceleration response (9 substructures × 3 groups). Then, the FFT is used to obtain the FRFs. Therefore, each group of excitation and acceleration responses generates an averaged frequency spectrum. By using the target frequency, $m^{\#}$ is calculated by Equation 4 and m^{*} is calculated by Equations 8–10. The calculated values are listed in Table 6.

5.1.3 | Damage identification

The damage identification results are shown in Figure 17. First, the initial FE model is used, and the corresponding damage identification results are shown in Figure 17. It can be seen that errors of damage identification are relatively large. Then the tuned FE model is used, and even if there still are errors between the experimental structural frequencies and the tuned FE model frequencies, these errors are much smaller. The damage identification results computed using the tuned FE model are more precise; see Figure 17. The accuracy of the proposed method depends thus on the precision of the FE model, and to obtain less errors, a tuned FE model should be used. Furthermore, when the direct virtual mass estimation method is used ($m^{\#}$), Substructures 3 and 4 can be wrongly identified as damaged. However, the improved estimation method (m^{*}) better identifies the damage of all substructures.

5.2 | Truss model

For a truss structure, the additional virtual mass added to a member significantly changes the local dynamic characteristics of the structure, and the damage can be judged directly by the value of the additional mass before and after the damage.

The experimental 3D structure is shown in Figure 18. It is supported at both ends, with a total length of 8 m, height of 0.45 m, and width of 0.56 m. There are 64 nodes and 184 members in total. The elastic modulus of the steel truss is $E' = 200$ GPa, Poisson's ratio is 0.2, and the density is $\rho = 7{,}800$ kg/m^3.
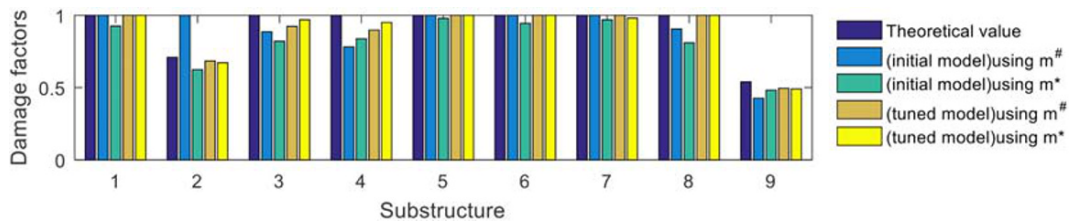

FIGURE 17 Damage identification results for the frame structure

FIGURE 18 Experimental 3D truss structure

The experimental equipment includes a modal hammer, a connector, and an acceleration sensor. As shown in Figure 19, the connector ensures that the sensor can be firmly connected to the round steel pipe. The tested diagonal rod is 90 cm in length, 2 cm in outer diameter, and 0.3 cm in wall thickness, and the moment of inertia of its cross-section is 5.97×10^{-9} m^4. The local damage of the member is simulated by cutting and thinning its middle part. As shown in Figure 20, half of the cross-section is removed on the length of 7.7 cm in the middle of the member, and the remaining sections are semicircular. The moment of inertia of the semicircular reduced cross-section is 5.89×10^{-10}m^4. The bending stiffness of the damaged 7.7 cm component is thus reduced to 0.0987 of the initial stiffness. According to the principle of the same displacement under the unit force of a single member in the span, the effective local damage of the entire member can be approximated as 0.318.

First, a knock test of the undamaged member was performed, as shown in Figure 19. The sampling frequency of the experiment was 20,000 Hz. The load excitation (Figure 21) and acceleration response (Figure 22) were obtained as functions of time. A Fourier transform was then applied to obtain the response curve in the frequency domain (Figure 23).

FIGURE 19 Undamaged member

FIGURE 20 Damaged member

FIGURE 21 Time history of modal force hammer excitation
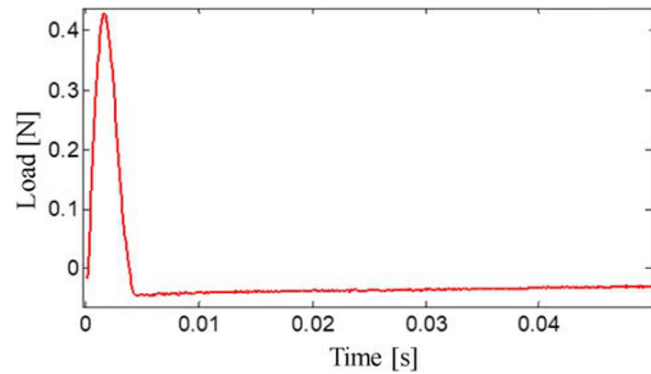
FIGURE 22 Time history of acceleration response
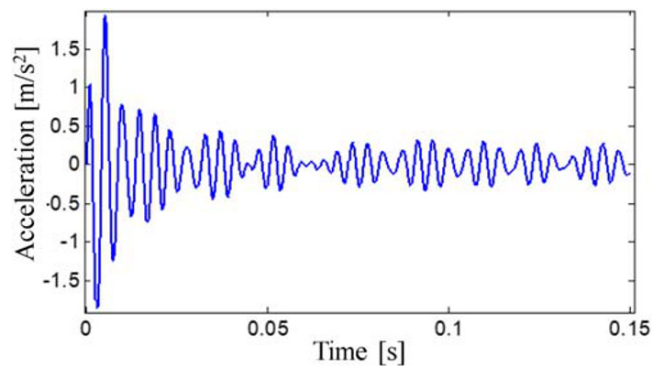
FIGURE 23 Frequency response curve
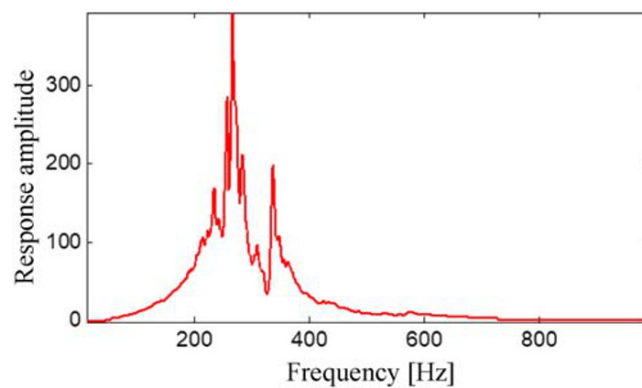
For $\omega^* = 85$ Hz, using the frequency response near 85 Hz in Figure 23, it was estimated that the virtual mass required was 3.48 kg. The same dynamic experiment was repeated on the damaged rod, as shown in Figure 20. For the same target frequency $\omega^* = 85$ Hz, the estimated additional virtual mass was 1.24 kg only. It can be clearly seen that the additional mass required after the damage was much smaller, which can be used to quickly and accurately determine that the structure has been damaged. Combined with the structural FE model, the identified damage factor for the modified member is 0.243. Compared with the actual damage factor of 0.318, it is within the acceptable engineering range.

6 | CONCLUSION

In this paper, the method of estimating the additional mass according to the target natural frequency for damage identification is proposed. The effectiveness of the proposed method is verified by a numerical simulation of a simply supported beam and experiments of a plane frame and a truss structure. The conclusions drawn from this work are as follows:The proposed method uses frequencies from around the target frequency only. Therefore, besides impulse, also

a simple harmonic or a narrow spectral excitation can all serve the virtual mass estimation methods, which can be widely used in practical engineering.

1. The proposed additional mass estimation methods include direct and improved approaches: the direct estimation method directly calculates the virtual additional mass according to one FRF point only, the target frequency, in the entire frequency response. Therefore, it is highly efficient for performing calculations. The improved method utilizes also frequencies around the target frequency, and thus, it is highly precise.
2. For the truss structure, because the additional virtual mass significantly affects the local dynamic characteristic of the tested member, the value of the additional mass can be directly used to determine whether the tested member is damaged. For the frame and beam structures, it is necessary to apply additional virtual masses to the structure at multiple positions to determine the degree and position of the damage.
3. A limitation of the proposed method is the fact that the excitation should be applied and the response measured in the same DOF, so that the experimental conditions need to be well designed. Moreover, the method requires the excitation to be measured, so that it cannot be applied with ambient excitation. The latter limitation is an important path for further research.

ORCID

Jilin Hou https://orcid.org/0000-0002-3554-7036
Zhenkun Li https://orcid.org/0000-0002-1444-6017
Łukasz Jankowski https://orcid.org/0000-0002-9773-0688

REFERENCES

1. Fan W, Qiao PZ. Vibration-based damage identification methods: A review and comparative study. *Struct Health Monit*. 2001;10(1): 83-111.
2. AnY, Chatzi E, Sim SH, Laflamme S, Blachowski B, Ou J. Recent progress and future trends on damage identification methods for bridge structures. *Struct Control Health Monit*. 2019;10(10):1–30, e2416. https://doi.org/10.1002/stc.2416
3. Weng S, Zhu H, Xia Y, Li J, Tian W. A review on dynamic substructuring methods for model updating and damage detection of large-scale structures. *Adv Struct Eng*. 2020;23(3):584-600. https://doi.org/10.1177/1369433219872429
4. Zhang QX, Jankowski L, Duan ZD. Simultaneous identification of excitation time histories and parametrized structural damages. *Mech Syst Signal Process*. 2012;33:56-68.
5. Xing Z, Mita A. A substructure approach to local damage detection of shear structure. *Struct Control Health Monit*. 2012;19(2):309-318.
6. Zhang DY, Yang Y, Wang TQ, et al. Improving substructure identification accuracy of shear structures using virtual control system. *Smart Mater Struct*. 2018;27(2):1-1.
7. Sampaio RPC, Maia NMM, Silva JMM. Damage detection using the frequency-response-function curvature method. *J Sound Vib*. 1999; 226(5):1029-1042.
8. Maia NMM, Silva JMM, Almas EAM, et al. Damage detection in structures: from mode shape to frequency response function methods. *Mech Syst Signal Process*. 2003;17(3):489-498.
9. Huang Q, Xu YL, Li JC, Su ZQ, Liu HJ. Structural damage detection of controlled building structures using frequency response functions. *J Sound Vib*. 2012;331(15):3476-3492.
10. Shi ZY, Law SS, Zhang LM. Damage localization by directly using incomplete mode shapes. *J Eng Mech*. 2000;126(6):656-660.
11. Zhou J, Li Z, Chen JL. Damage identification method based on continuous wavelet transform and mode shapes for composite laminates with cutouts. *Compos Struct*. 2018;191:12-12, 23.
12. Hearn G, Testa RB. Modal analysis for damage detection in structures. *J Struct Eng*. 1991;117(10):3042-3306.
13. HouR, Xia Y, Zhou X. Structural damage detection based on l_1 regularization using natural frequencies and mode shapes. *Struct Control Health Monit*. 2017;25(3):1–17, e2107.
14. SinghMP, Elbadawy MZ, Bisht SS. Dynamic strain response measurement-based damage identification in structural frames. *Struct Control Health Monit*. 2018;25(7):1–21, e2181.
15. Dinh-Cong D, Vo-Duy T, Nguyen-Thoi T. Damage assessment in truss structures with limited sensors using a two-stage method and model reduction. *Appl Soft Comput*. 2018;66:264-277. https://doi.org/10.1016/j.asoc.2018.02.028

16. Dinh-Cong D, Vo-Van L, Nguyen-Quoc D, Nguyen-Thoi T. Modal kinetic energy change ratio-based damage assessment of laminated composite beams using noisy and incomplete measurements. *J Adv Eng Comput*. 2019;3(3):452-463. https://doi.org/10.25073/jaec.201933.248

17. GuoHY, Li ZL. Structural multi-damage identification based on modal strain energy equivalence index method. *Intl Jf Struct Stabil Dynam*. 2014;14(07):1–17, 1450028.

18. WangY, Thambiratnam DP, Chan THT, Nguyen A. Damage detection in asymmetric buildings using vibration-based techniques. *Struct Control Health Monit*. 2018;25(2):1–19, e2148.

19. ZhaoY, Noori M, Altabey WA, Beheshti-Aval SB. Mode shape-based damage identification for a reinforced concrete beam using wavelet coefficient differences and multiresolution analysis. *Struct Control Health Monit*. 2017;25:(1):1–41, e2041.

20. Dinh-Cong D, Dang-Trung H, Nguyen-Thoi T. An efficient approach for optimal sensor placement and damage identification in laminated composite structures. *Adv Eng Softw*. 2018;119:48-59. https://doi.org/10.1016/j.advengsoft.2018.02.005

21. Dinh-Cong D, Pham-Toan T, Nguyen-Thai D, Nguyen-Thoi T. Structural damage assessment with incomplete and noisy modal data using model reduction technique and LAPO algorithm. *Struct Infrastruct Engr*. 2019;15(11):1-14. https://doi.org/10.1080/15732479.2019.1624785

22. Nalitolela NG, Penny JET, Friswell MI. A mass or stiffness addition technique for structural parameter updating. *Int J Anal Exp Modal Anal*. 1992;7(3):157-168.

23. Cha P, De Pillis L. Model updating by adding known masses. *Int J Numer Methods Eng*. 2001;50(11):2547-2571.

24. Dems K, Mroz Z. Damage identification using modal, static and thermographic analysis with additional control parameters. *Comput Struct*. 2010;88(21–22):1254-1264.

25. Dinh HM, Nagayama T, Fujino Y. Structural parameter identification by use of additional known masses and its experimental application. *Struct Control Health Monit*. 2012;19(3):436-450.

26. Lee ET, Eun HC. Damage identification of a frame structure model based on the response variation depending on additional mass. *Eng Comput*. 2015;31(4):737-747.

27. Kolakowski P, Wiklo M, Holnicki-Szulc J. The virtual distortion method—a versatile reanalysis tool for structures and systems. *Struct Multidiscipl Optim*. 2008;36(3):217-234.

28. Zhang D, Li S, Li H. Adaptive substructure identification for shear structures with virtual control system. *Mech Syst Signal Process*. 2019;121:426-440. https://doi.org/10.1016/j.ymssp.2018.11.025

29. Hou JL, Jankowski L, Ou JP. Structural damage identification by adding virtual masses. *Struct Multidiscip Optim*. 2013;48(1):59-72.

30. HouJL, An YH, Wang SJ, et al. Structural damage localization and quantification based on additional virtual masses and Bayesian theory. *J Eng Mech*. 2018;144(10):1–9, 04018097.

31. Hou J L, Jankowski L, Ou J P. Structural health monitoring based on combined structural global and local frequencies. *Math Probl Eng* 2014:1–13, Article ID 405784.